BULLETIN OF THE POLISH ACADEMY OF SCIENCES
TECHNICAL SCIENCES, Vol. 70(2), 2022, Article number: e140517
DOI: 10.24425/bpasts.2022.140517

A novel revolutionary substantial transformative control technique for solar fed-full bridge converter based energy stabilization for grid connected applications

UMAMAHESWARI S.[1]*, KARTHIGAIVEL R.[1], SATHEESH KUMAR G.[2], and VENGADACHALAM N.[3]

[1] PSNA College of Engineering and Technology, Kothandaraman nagar, Dindigul – 624622 Tamil Nadu, India
[2] SSM Institute of Engineering and Technology, Dindigul-Palani Highway, Dindigul – 624002 Tamil Nadu India
[3] Malla Reddy Engineering College for Women, Maisammaguda, Dhulapally, Secunderabad – 500100 Telangana, India

Abstract. Nowadays, there is a need to increase the continuous usage of the power electronic converters like AC-DC, DC–DC, and DC–AC based on various applications like mobile charge controller and telecom base station. Also, for power stability control, these converters are utilized in the renewable energy system (RES). The output cannot be stable for a longer duration due to the inappropriate switching pulse and continued usage of the converter. For resolving the above issues, the soft-switching technique is implemented in the proposed system for controlling both converter and inverter for proper energy stabilization during the continuous operation of devices. The main objective of this work is to improve the solar power system using high voltage gain DC / DC converter. Similarly, an inverter delivers the continuous AC power to the grid system without any fluctuations. The revolutionary substantial transformative control (RSTC) technique has been employed to monitor and control the converters used in this system. The additional advantage of this system is battery-based energy management, which is only utilized under necessary conditions. During the initial stage, RSTC will track the solar power, and it compares with the reference voltage and produces the appropriate pulse to the converter switch. Based on the switching pulse, the full-bridge converter (FBC) will also enhance the DC voltage by providing the constant voltage for the grid-connected inverter system. Secondly, the proposed RSTC controller will be monitoring voltage amplitude and frequency of grid power system. If any variation appears due to source power fluctuation, the controller will recognize it and automatically vary the pulse width modulation (PWM) of an inverter and compensate the grid power. The design analysis and operating approaches of the proposed converter are verified by MATLAB / Simulink 2017b. The performance analysis has been done with various parameters like total harmonics distortion (THD), steady-state error and converter efficiency.

Key words: high boost full-bridge converter; battery energy storage system (BESS); revolutionary substantial transformative control (RSTC) technique.

1. INTRODUCTION

In recent years, several studies have focused on the utilization of solar, wind, water, biomass, and renewable energy gas, for electricity generation. These RES are difficult to connect to the grid system because the power generation from renewable energy systems is not constant. For maintaining the stability of the renewable energy generation, a high-performance converter with an advanced PWM control is needed. In this proposed system, the full bridge converter with soft switching techniques is utilized to stabilize the renewable energy generation. The proposed method is designed with a grid-connected photovoltaic (PV) system, and battery-based energy management is also implemented; the effective operation of a proposed model is represented in Fig. 1.

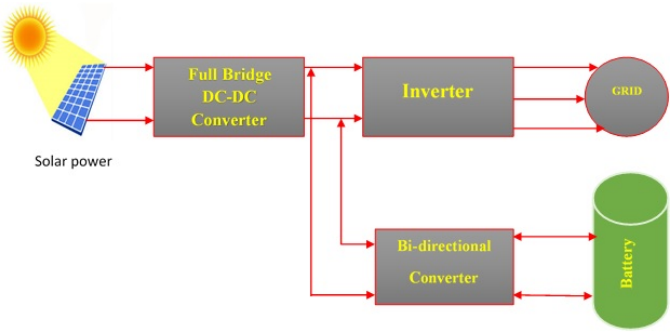

Fig. 1. Functional block diagram for the grid-connected solar power generation

The proposed PV system needs a high boost full-bridge converter and inverter for the stable energy transformation of grid-connected applications. The power converter exchanges the power between PV and grid power system. These power converters should achieve a stable energy transformation based on

*e-mail: umasubbaiah@gmail.com

Manuscript submitted 2021-08-12, revised 2021-09-25, initially accepted for publication 2021-11-12, published in April 2022.

two main functions: Firstly, ensure the maximum power point tracking (MPPT), from the PV array which is generated based on the atmospheric and load conditions.

This condition is analyzed using RSTC-based MPPT, controller will provide the PWM to a FBC and stabilize the DC power based on the tracking signal. The second function is converting DC voltage into AC voltage by using the inverter. The transformed AC voltage should always be the same as the grid voltage and should consider peak amplitude and frequency of the waveform. The proposed RSTC controller will maintain the above parameters consistently.

The functional block diagram of Solar fed H-bridge converter with a grid-connected inverter is shown in Fig. 1. The prime function of FBC is to stabilize solar power and provide constant input for the grid-connected inverter. The proposed RSTC method utilizes the active tracking of the maximum potential in the MPP system, which will initially improve solar power stability. The implementation of the proposed model will increase the solar voltage up to ten times for grid-tie conditions. The main goal is to accomplish a lower response time and higher efficiency in the MPPT system.

The second stage is the function of the inverter using RSTC. To ensure efficient use of grid-connected solar power, the inverter is designed to get energy conversion and adaptation functions between the source and the grid voltage. The conversion principle in these inverters is to use RSTC technique to provide a stable sinusoidal voltage with the lowest THD and to maintain the peak output voltage of 620V AC to the grid system by providing the proper pulse to the inverter. The proposed RSTC will always ensure low THD, and it will maintain the sinusoidal waveform of the inverter output under dynamic conditions.

The third stage of the process is battery management for the continuous power delivery to the grid system. The bi-directional converter-based BESS is used. The proposed work is significant for its computational energy scheduling solutions for grid-tied micro grids in a highly stochastic situation, which includes a battery management system. The bi-directional converter will maintain the charging/discharging state of a battery. The additional advantage of a bi-directional converter is that it will work in buck/boost mode of operations. During the charging condition, it will work in the buck mode to maintain 12 V for charging the battery. If the solar power output reduces to the value between (0-8) V, the RSTC controller provides the modified switching operation of the bi-directional converter. During this condition, the converter will act in boost mode while maintaining the 620V in the DC bus system. The RSTC technique will maintain and control the battery power. The proper implementation of all three stages is required to achieve a high-performance converter and inverter with a fast dynamic response with low THD and pure sine wave in inverter output voltage, which is more suitable for solar stability power generation-based grid-tie applications. The proposed RSTC technique will monitor and control all the proposed model parameters. The main contribution of this work is to maintain the output voltage at different solar irradiance and quick energy compensation of the system.

2. LITERATURE SURVEY

The proposed system needs to identify the drawbacks of the conventional approaches that are given below for improving the solar-based FBC with the grid-connected inverter.

An implemented single-phase isolated DC–AC converter is applicable for low power solar power stabilization. In the circuit, the principle of using two full-bridge cells placed on both sides of high-frequency transformer floating DC bus capacitors and working on a dual active bridge [1]. Full load range operation requirements of semi-dual active bridge and DC–DC converter for battery charging through multi-mode control strategy [2]. Phase shift control uses dual transformer-based switches with minimum power and half-bridge output, and the control law suggests various zero voltage switching (ZVS) and reduces current-related losses [3]. For bidirectional DC–DC converters with current-fed dual active bridges, it is recommended to use the extended duty cycle control model [4]. The current-fed power electronics topologies for wireless power transmission (WPT) systems and its analysis are based on charged electric vehicle applications [5]. The controlled transitional full-bridge (CTFB) and hybrid multilevel converter (HMC) are suitable for medium and high voltage applications [6–9].

The three phase asymmetric half-bridge (AHB) converter with torque ripple reduction and auxiliary MPPT algorithm are used to improve the voltage stability of the converter [10]. The aim of this system used is to improve the execution of the three-level converter and its control techniques based on its sophisticated function [11–15]. In this analysis, a full-bridge-modular multi-level converter (FB-MMC) has been utilized to stabilize DC voltage provided to grid-tie inverter for a continuous AC power flow. In this analysis, a full-bridge-modular multi-level converter (FB-MMC) is utilized for the stabilization of DC voltage provided to the grid-tie inverter for continuous AC power flow. An analysis of implemented ZVS techniques in FBC network zero and finite phase overlap operation [16–20].

The droop control technique has been used for the effective control of the hybrid system [21, 22]. A multi-input converter will actively utilize hybrid energy storage system (HESS) [23, 24]. Phase shift control is a significant control technique because of its easy implementation and stable performance in hybrid systems [25].

The output of the proportional integration (PI) controller creates the required grid to switch between full-bridge arms. Finally, the output generates the gate signal and supplies it to the converter to achieve DC voltage stabilization [26]. To improve conversion efficiency, the full-load operation performance under a multi-mode control strategy proposes a semi-double active bridge (sDAB) of DC–DC converter [27, 28]. The transformer-coupled dual input converter (TCDIC) can achieve MPPT and battery charge control while sustaining an appropriate voltage level at the load system [29]. Transformer-coupled boost semi-bridge converters are used for wind power stabilization. In contrast, bidirectional buck-boost converters are used for charge/discharge control from the PV generation system along with the battery [30–33]. battery management systems [BMS] are responsible for making the best use of a battery's remain-

ing energy. BMS systems protect batteries from deep discharge and over-voltage, which are caused by excessive fast charge and extreme high discharge current, to avoid overloading devices. From the analysis of conventional methods, various parameters need to be improved, such as THD, steady-state error, and efficiency. The proposed grid-connected solar power generation system ensures the improvement in the above parameters to improve the system's performance.

3. MATERIALS AND METHODS

The proposed system includes two primary devices called DC–DC converter and inverter, connected between the photovoltaic array and the AC grid system. The full-bridge DC–DC converter is initially controlled by RSTC technique, which computes the maximum power and ensures DC power stability and then the inverter provides continuous power to the grid system. This condition will be achieved by using the RSTC controller, which consists of monitoring frequency, amplitude, and sinusoidal voltage. If there is any variation in the above parameters, the controller will provide appropriate PWM to the inverter and maintain the desired values of those parameters. The controller also reduces the harmonic distortion in the output waveforms. In the third stage of the process, battery-based energy management is implemented in this proposed system. If solar power efficiently provides the energy, the bi-directional converter will regulate and charge the battery.When the source power goes low, the bi-directional converter will be discharging the voltage from the battery and compensate the grid power.

The block diagram of RSTC technique-based solar power stabilization is shown in Fig. 2. The proposed RSTC technique monitors and controls the battery power under necessary conditions. The purpose of these techniques is to optimize grid power under source power fluctuating conditions.

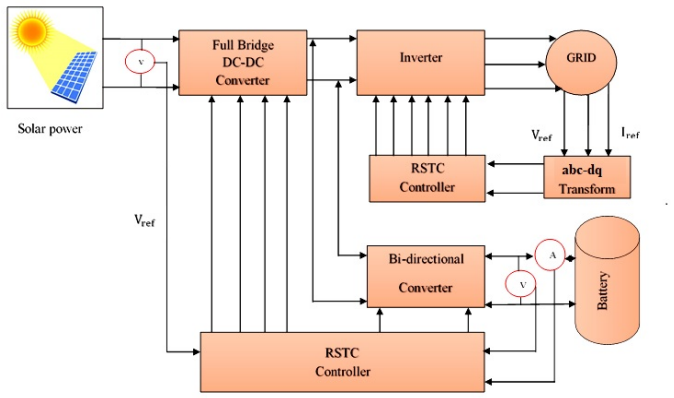

Fig. 2. Proposed block diagram for RSTC technique-based solar power stabilization

3.1. Design of PV array

Photovoltaic solar cells are made of P-type and N-type semiconductor material. The solar cell has a voltage based on solar irradiance. The solar power equivalent circuit is shown in Fig. 3. It contains a diode, series resistor and shunt resistor in parallel with current generator. Shunt resistance refers to the leakage current flowing through the ground, which is usually very high, about 1000 Ω. The series resistance refers to the internal resistance tracks associated with the solar cell, and the series resistance is 0.001 Ω. A single solar cell generates a low voltage typically (0.5–0.7) V; therefore, solar cells are arranged either in serial or in parallel manner to make an array of solar cell. The proposed system has utilized four parallel combinations of the solar panel.

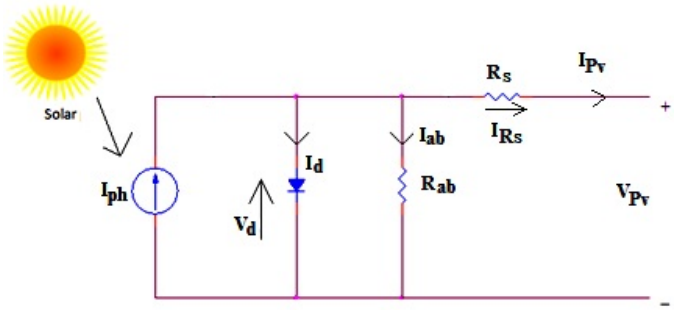

Fig. 3. PV cell equivalent circuit

The governing equation for this equivalent circuit is currently designed using Kirchhoff's current law I_{pv}.

$$I_{pv} = I_{ph} - I_d - I_{ab}\,, \tag{1}$$

$$I_d = I_{d0}\left[\exp\left(\frac{V_{pv}+I_{Rs}}{nV_t}\right)-1\right], \tag{2}$$

$$V_t = \frac{KT_c}{Q}\,, \tag{3}$$

where,

I_{pv} – current through the load,
I_{ph} – solar cell current,
I_d – current through the diode,
I_{ab} – current in the parallel resistance,
n – diode ideality factor,
I_{d0} – diode reverse current,
V_t – thermal voltage depending on the cell temperature,
V_{pv} – solar cell voltage,
K – Boltzmann's constant,
Q – elementary charge,
T_c – instantaneous solar cell temperature.

While equating the shunt current as $I_{ab} = \left(\frac{V_{PV}+I_{Rs}}{R_{ab}}\right)$ by combining the above shunt current equation, the complete governing equation of single diode (cell) equation is expressed as below:

$$I_{PV} = I_{Ph} - I_{d0}\left[\exp\left(\frac{V_{pv}+I_{Rs}}{nV_t}\right)-1\right] - \frac{V_{PV}+I_{Rs}}{R_{ab}}\,. \tag{4}$$

The five parameters I_{Ph}, I_{d0}, I_{Rs}, R_{ab} and in (4), which are equivalent circuit models of all single diodes.

3.1.1. MPPT control

The MPPT technique analyses the operating point of the solar panel. Also, it will recognize the MPP with quick response and control to the converter. The proposed RSTC-MPPT system will measure the solar power curve alienated in two sides, left and right side MPPT. The deviation in current and voltage are analyzed to get closer to the point of operation. Then specific areas of activity are formulated for solar PV panels and fine-tuned reference voltages. Based on the tracking of solar power, the RSTC controller will vary the PWM of the FBC, as represented in Fig. 4. The fill factor (FF) is the ratio between maximum power of solar panel and output at open-circuit voltage (V_{OC}) and short-circuit current (I_{SC}). The FF determines the MPP obtained from the photovoltaic panel. The RSTC controller measures the above two parameter values.

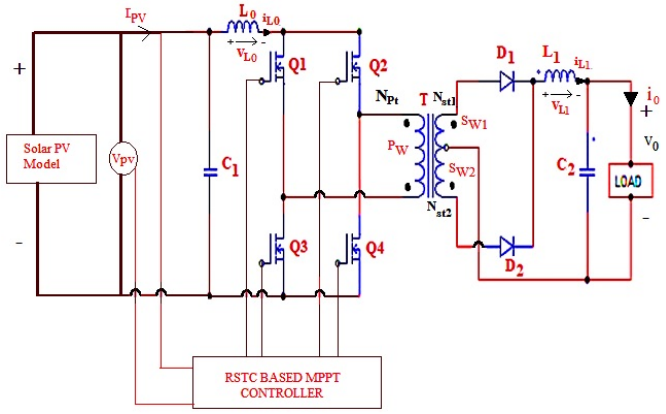

Fig. 4. RSTC based DC–DC converter

3.1.2. RSTC-MPP tracking

The RSTC technique-based MPPT is executed to track the MPP of the SPV array. The proposed method will evaluate the V-I characteristic of the PV system, defined by the equation of $\left(\frac{\partial P_{pv}}{\partial V_{pv}} = 0\right)$, which are the left and right side of the MPPT. The formulation of the proposed controller based on MPPT equations is given below:

$$P_{pv} = V_{pv} \times I_{pv}\,. \tag{5}$$

Applying the chain rule for the derivative of the generated solar output, which is expressed in 6)

$$\frac{\partial P_{pv}}{\partial V_{pv}} = \frac{[\partial\,(V_{pv} * I_{pv})]}{\partial v_{pv}}\,. \tag{6}$$

At MPP tracking system,

$$\frac{\partial P_{pv}}{\partial V_{pv}} = 0. \tag{7}$$

The above formula can be written as the array voltage V_{pv} and the array current I_{pv} as a conversionwhich is given in below in (8)

$$\frac{\partial I_{pv}}{\partial V_{pv}} = -\frac{I_{pv}}{V_{pv}} \text{ at MPP}, \tag{8}$$

$$\frac{\partial I_{pv}}{\partial V_{pv}} > -\frac{I_{pv}}{V_{pv}} \text{ at the left of MPP}, \tag{9}$$

$$\frac{\partial I_{pv}}{\partial V_{pv}} < -\frac{I_{pv}}{V_{pv}} \text{ at the right of MPP}. \tag{10}$$

The RSTC-MPPT regulates the PWM control signal to the full bridge converter until the condition, $\left(\frac{\partial I_{pv}}{\partial V_{pv}}\right) + \left(\frac{I_{pv}}{V_{pv}}\right) = 0$ is satisfied. The proposed RSTC-MPPT algorithm provides direct duty cycle control of the converter with a simple adjustment. The RSTC controller provides a direct duty cycle control, which provides an excellent stability feature and high energy utilization due to the small effect of noise and fewer ripples produced in the output. The sophisticated PWM pulse to the converter will improve the DC voltage with fewer distortions. The proposed RSTC has excellent tracking performance that can be achieved under dynamic conditions with small oscillations around the optimal operating point. Hence, solar power will achieve stabilization through the four stages of the FBC operation described in the below section.

3.2. Design and operation of full-bridge converter

Figure 5 illustrates the design and operation of a proposed converter, which consists of converter switches (Q1-Q4), input filter (C_1), isolation center-tapped transformer T, full wave rectifier diodes (D_1 and D_2) and an output filter (L_1C_2). For analyzing the performance of the converter, the following is assumed: MOSFET switch is ideal; based on the PWM variation, the inductor L_0 provides an improved continuous current, and capacitor C_2 will maintain the constant output voltage of a converter.

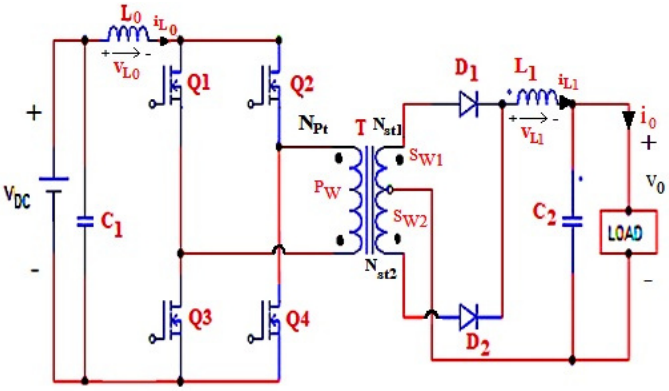

Fig. 5. Schematic diagram of full-bridge converter

The solar system provides the source voltage (V_{dc}) to the converter and the system output is defined as (V_o). The inductor L_0 will increase the solar voltage to the required output. The capacitor C_1 maintains the source voltage, and the capacitor C_2maintains the load voltage. The FBC contains MOSFET switches Q1, Q2, Q3, and Q4. The two switches work simultaneously and provide voltage to the primary winding (P_W) of the transformer in every half-cycle. The center tap secondary winding (S_{W1} and S_{W2}) provides step-up voltage to the full-wave

rectifier (D_1 and D_2), which provides the DC voltage (V_o) to the load. The output filters (L_1 C_2) maintain the constant output with less ripple ratio.

Mode 1: In the mode 1 operation, all switches (Q1, Q2, Q3, and Q4) are turned "ON", as a result, the energy is stored in the inductor L_0, because its voltage is constant (inductor L_0 voltage is equal to V_{dc}). During this period, the inductor current linearly increases. The transformer primary winding (P_W) is shorted because the Q1-Q3 and Q2-Q4 carry half of the input current ideally. The output current of a rectifier is freewheeling through D2, but the capacitor C_2 discharges the voltage to the load, as shown in Fig. 6.

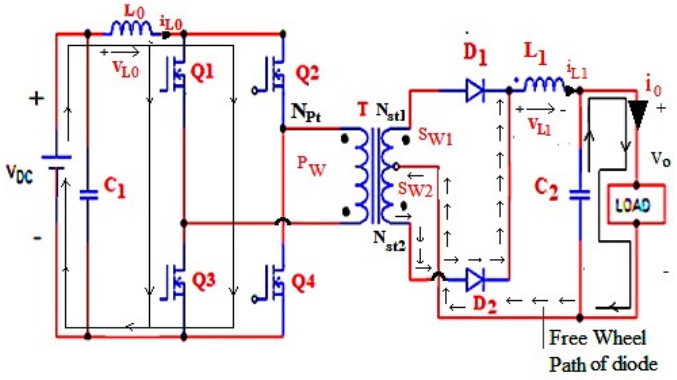

Fig. 6. Mode 1 operation when all switches are "ON"

Mode 2: The switches Q1 and Q4 are closed in this mode and power is transferred from PV to load. This happens due to the stored energy of the inductor L_0 which will be flowing through the Q1 and Q4 switches. Due to this, the transformer primary winding P_W and secondary S_{W1} are energized, and the energy will be flowing through the diode D_1 to the load system. The energy flowing path is represented in the Fig. 7.

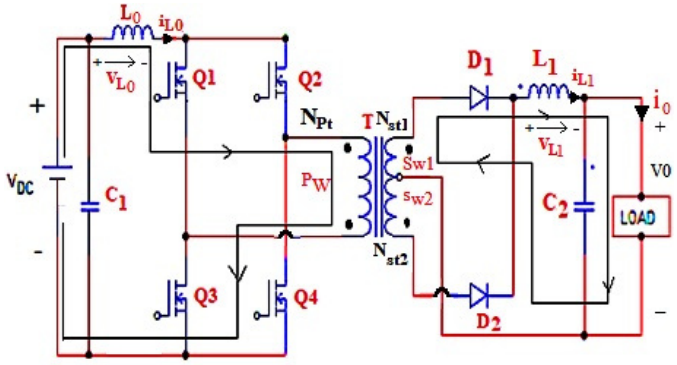

Fig. 7. Mode 2 operation when Q1 and Q4 are "ON"

Mode 3: In this mode, all the switches (Q1, Q2, Q3, and Q4) are turned to the "ON" state. As a result, the energy is stored in the inductor L_0, because its voltage is constant (inductor L_0 voltage is equal to V_{dc}). During this period, the inductor current linearly increases; thus, freewheeling will occur through the diode D_1 and the capacitor C_2 the voltage will be discharged to the load system, which is shown in Fig. 8.

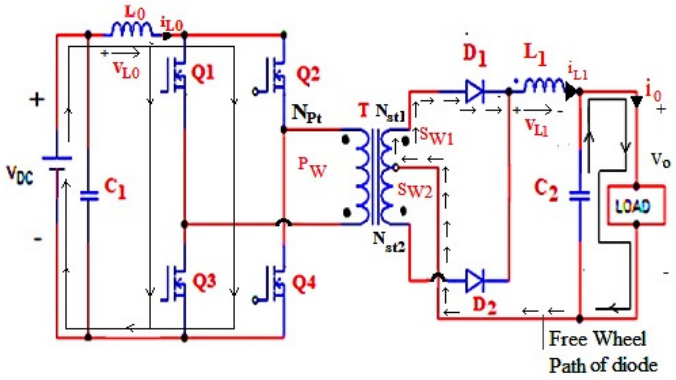

Fig. 8. Mode 3 operation all switches are in "ON"

Mode 4: In the mode 4 operation, the switch Q2 and Q3 are in ON state. During this condition, the inductor L_0 storage energy will be flowing through the Q2 and Q3 switches; due to this, the transformer primary winding P_W and secondary S_{W2} are energized, and the energy will be flowing through the diode D_2 to the load system. The energy flowing path is represented in the circuit diagram, as in Fig. 9.

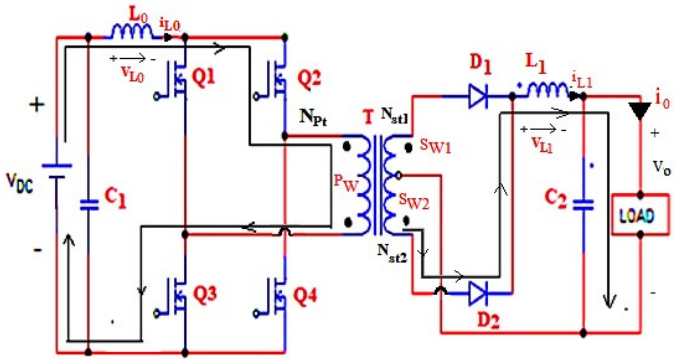

Fig. 9. Mode 4 Operation Q2 and Q3 are in "ON"

Ideal waveform for one switching cycle operation of FBC is shown in Fig. 10. The modes of a proposed full bridge circuit are summarized through the above ideal waveform for the simplification of analysis. In the above Fig. 10, it is clearly shown that the mode (1&3) and mode (2&4) operations based corresponding waveform of input inductor (L_0) and output filter (L_1, C_2) are described.

Based on the switching pulses to the FBC, the source (PV) voltage will be increased and stabilized. All the switches are in ON condition during the mode 1&3. In this condition, input inductor (L_0) is in charging condition, which is highlighted in the triangle shape of the waveform, the output inductor current (L_1) decreases and freewheeling will happen. This condition will be highlighted in a triangle shape in IL_1, and also the output capacitor C_2 is discharged. During the (2&4) Q1-Q4 and Q2-Q3 are in "ON" state with different half-cycle operations. In this state, the input inductor (L_0) is discharging in condition, and power transfer will happen through the Transformer (T) and diode (D1&D2) and also the output inductor current (L_1) in-

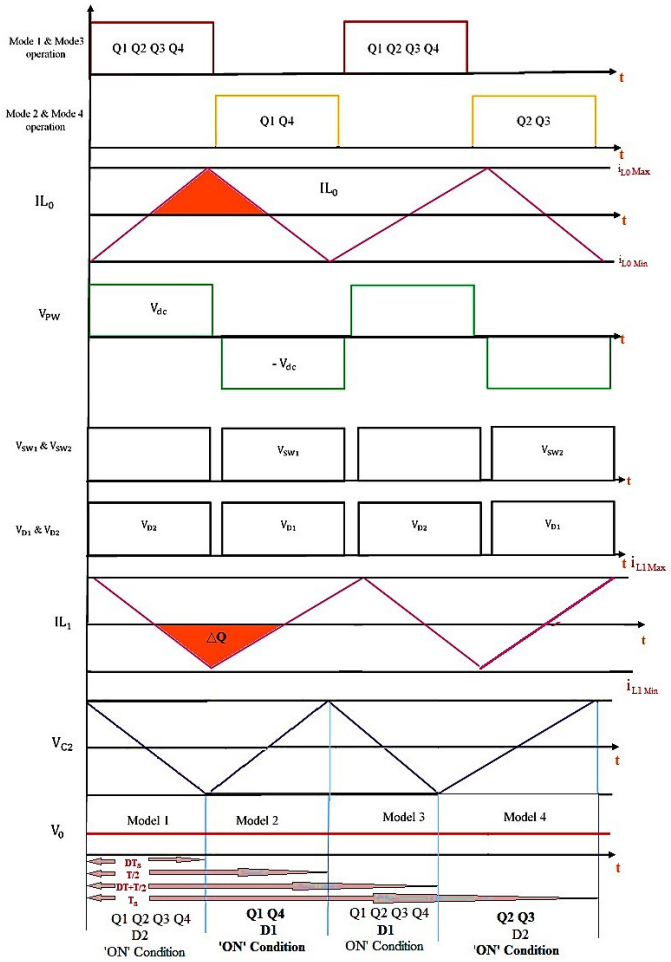

Fig. 10. Ideal waveform for FBC

creases and capacitor C_2 is in discharging condition particular waveforms are represented in Fig. 10. The common switching operations for all the four intervals of the FBC converter are summarized as below.

3.2.1. Mode 2 and 4 operations

When the switches Q1–Q4 and Q2–Q3 are in "ON" state during different half-cycle operations, the charged inductor current will be drawn through the switch (Q1–Q4 or Q2–Q3) based on the modes of operation. During this condition, energy will be transferred from PV to load via transformer, diode, and filter circuit, so this mode is known as "power transfer mode", which is represented in Figs. 7 and 9. Figure 10, characterizes the conducting device during this interval. The following formula can be obtained from Fig. 7.

$$V_{dc} \leq V_o \,. \tag{11}$$

For analyzing the step-up transformer voltage, the secondary winding ratio should be evaluated, which is expressed below in (12):

$$V_{SW1} = \left(\frac{N_{St1}}{N_{Pt}}\right) V_{dc}; \qquad V_{SW2} = \left(\frac{N_{St2}}{N_{Pt}}\right) V_{dc} \,. \tag{12}$$

The total voltage across the inductor L_1,

$$V_{L1} = \left(\frac{N_{St1}}{N_{Pt}}\right) V_{dc} - V_o \,. \tag{13}$$

where,

I_{pv} – current through the load,
V_{dc} – the source DC voltage provided to the converter,
V_{PW} – primary transformer voltage,
V_{SW1}, V_{SW2} – the transformer secondary voltage,
N_{Pt}, N_{St1}, N_{St2} – primary and secondary transformer turns ratio,
V_{L0} – the input inductor voltage,
V_{L1} – the output inductor voltage,
V_o – output load voltage,
i_{L0} – input inductor current,
i_1 – output inductor current.

The ratio of the i_{L0} is

$$\frac{di_{L0}}{dt} = \frac{V_{L0}}{i_{L0}} = \left(\frac{N_{St1}}{N_{Pt}}\right) V_{dc} - \frac{V_o}{(L_1 + C_2)} \,. \tag{14}$$

The current variation of the inductor during ON condition is

$$(\Delta i_{L0})_{\text{ON}} = \left\{ n V_{dc} - \frac{V_o}{L_0} \right\} (\Delta t)_{\text{ON}} \,, \tag{15}$$

$$(\Delta i_{L0})_{\text{ON}} = \left\{ n V_{dc} - \frac{V_o}{L_0} \right\} D T_s \,, \tag{16}$$

where, $n = \left(\frac{N_{St1}}{N_{Pt}}\right) = \left(\frac{N_{St2}}{N_{Pt}}\right)$ and the PWM of the switch $D = \frac{T_{\text{ON}}}{T_s}$ for cyclic intervals of switches.

3.2.2. Mode 1 and Mode 3 operations

In these modes all the switches are in "OFF" condition, so power is not transmitted from PV to load. During this condition, inductor iL_1 current linearly decreases; thus, freewheeling will occur through the diode D_2 and D_1 based on mode 1 and mode 3 operations, which are represented in Fig. 6 and Fig. 8.

The voltage variation of the inductor L_1 is expressed as

$$\frac{di_{L1}}{dt} = \frac{-V_o}{L_1} \,. \tag{17}$$

During the half-cycle period of the switches, the variation in L_1 the inductor current is assumed as

$$(\Delta i_{L1})_{\text{OFF}} = \frac{-V_o}{L_1} (\Delta t)_{\text{OFF}} \,, \tag{18}$$

$$T_{\text{OFF}} = \left(\frac{T_s}{2}\right) - T_{\text{ON}} = 0.5\, T_s - T_{\text{ON}} \,, \tag{19}$$

$$T_{\text{ON}} = 0.5\, T_s - T_{\text{ON}} \,. \tag{20}$$

The T_{OFF} and T_{ON} is the half-cycle period of the switches in mode 2 and mode 4, respectively.

In (20), 0.5 denotes the switching delay of the inverter to turn "OFF" and "ON" between the modes of operations. The deviation of the inductor current is obtained by (18), which is given as the substitution (19),

$$(\Delta i_{L1})_{\mathrm{OFF}} = \frac{-V_o}{L_1}(0.5-D)T_s\,. \tag{21}$$

Change of inductor current on the output side is zero during the stable half period $\left(\frac{T_s}{2}\right)$ is given by

$$(\Delta i_{L1})_{\mathrm{ON}} + (\Delta i_{L1})_{\mathrm{OFF}} = 0. \tag{22}$$

By substituting (14) and (19) in (20):

$$\left\{\frac{(nV_{dc}-V_o)\,D_{T_s}}{L_1}\right\} + \left\{\frac{(0.5-D)\,V_oT_s}{L_1}\right\} = 0. \tag{23}$$

Solving (23) results in

$$V_o = 2DnV_{dc}\,. \tag{24}$$

From (24), it is clear to determine that the gain voltage is obtained by varying the switching DT_s switching cycle of the converter with the constant switching frequency of 5 kHz. The inductor L_1 will reduce ripple current to its appropriate value. In addition, the inductor current increases linearly, which is expressed by

$$(\Delta i_{L1})_{\mathrm{ON}} = \left\{nV_{dc} - \frac{V_o}{L_1}\right\}(\Delta t)_{\mathrm{ON}}\,, \tag{25}$$

$$(\Delta i_{L1})_{\mathrm{ripple}} = \left\{nV_{dc} - \frac{V_o}{L_1}\right\}T_{\mathrm{ON}}\,. \tag{26}$$

Similarly, the inductor current reduces as per (25) during D_{T_s} to T_s, in this period, all the switches are in "ON" state.

$$i_{L1,\min} - i_{L1,\max} = \frac{-V_o}{L_1}(0.5-D)T_s\,, \tag{27}$$

$$(\Delta i_{L1})_{\mathrm{ripple}} = \frac{V_o}{L_1}(0.5-D)T_s\,. \tag{28}$$

The output of L_1 is provided in the below equation:

$$L_1 = (0.5-D)\frac{V_oT_s}{(\Delta i_{L1})_{\mathrm{ripple}}}\,. \tag{29}$$

In mode 2 and mode 4 operations, the output inductor current i_{L1} is shown in Fig. 10. The DC ripple voltage responsible for the output is obtained from the deviation

$$\Delta V_o = \frac{\Delta Q}{C_2}\,, \tag{30}$$

where ΔQ is the i_{L1} the inductor in charging state and ΔV_o is the amplitude of the output voltage. In Fig. 10, the triangle area represents the positive inductor current, which is equated as

$$\Delta Q = \left\{\frac{\frac{1}{2}\left(\frac{T_s}{4}\right)(\Delta i_{L1})}{2}\right\}. \tag{31}$$

The limitation between the CCM and the DCM can be accomplished when the inductor current i_{L1} arrives at zero toward the end of the OFF condition. The normal current during the limit state of the inductor is given in (32),

$$i_{L1} = i_0\left(\frac{\Delta i_{L1}}{2}\right). \tag{32}$$

The ripple voltage of the FBC is reduced by the capacitor C_2 which is expressed in the (33) and the stabilized DC voltage is given to both inverter and battery charger.

$$C_2 = \left\{\frac{T_si_{L1}}{8}(\Delta V_o)_{\mathrm{ripple}}\right\}. \tag{33}$$

3.3. Battery energy storage system

The essential requirement of the BESS is to meet the required load voltage provided to the grid system. Based on this, the boosting operation of the bi-directional converter will improve the battery voltage. When the renewable system is not sufficient to run the load system, the battery-based energy storage system will compensate for the load. If the renewable system generates sufficient power to run the load, the battery is in a charging condition. In this condition, the bi-directional converter will act like a buck converter. The charging and discharging of a battery are computed by using (34) and this condition is controlled by the proposed RSTC controller. Figure 11 shows the circuit diagram of a bi-directional converter.

$$B_a(t) = B_a(t+1) + \big(B_a(t-1) + B_a(t-2)\big)\cdot C_{\mathrm{bat}}. \tag{34}$$

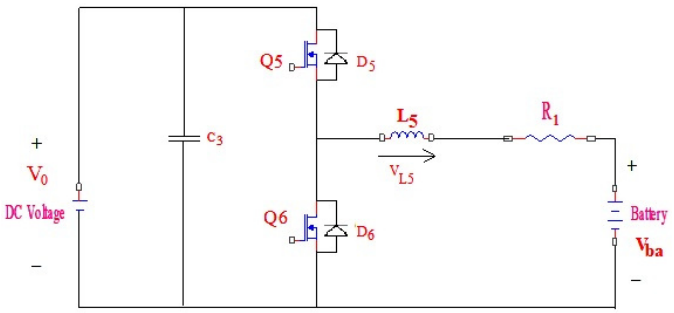

Fig. 11. Bi-directional DC–DC converter

During the battery charging mode, the Q5 switch turns to "ON", Q6 turns to "OFF", and the diode D_6 is in the reverse state. In this condition, the L_5 the inductor current is charged up linearly, also the capacitor C_3 is charged, and the resistance R_1 will drop the voltage, which is adequate for the charging of the battery V_{ba}.

When discharging, the Q6 switch turns to "ON", Q5 turns to "OFF", the current in L_5 is reduced to zero, and then charges polarity. In this state, the voltage across the filtering inductor L_5 is expressed as $V_{L5} = -V_0 + V_{ba}$. When both switches are turned off, the diode D_5 starts conducting. At this stage, the L_5 inductor voltage is expressed as $V_{L5} = V_0 - V_{ba}$. In this state, L_5 is discharging and flows through the diode D_5, the capacitor C_3 will reduce the ripple voltage across V_0 during the discharging condition.

The state of charge (SOC) depends on the power supplied by the full bridge DC–DC converter, which has been computed by employing the following conditions:

(i) For charging mode,

$$\mathrm{SOC}(t) = \mathrm{SOC}(t+1) + \frac{B_{\mathrm{bat}}(t)\, B_{\mathrm{charing}}}{P_N} \times 100. \tag{35}$$

(ii) For discharging mode,

$$\mathrm{SOC}(t) = \mathrm{SOC}(t-1) + \frac{B_{\mathrm{bat}}(t)\, B_{\mathrm{discharging}}}{P_N} \times 100, \tag{36}$$

where, $\mathrm{SOC}(t)$ is a charging and discharging of a battery, which will be analyzed with the estimated battery capacity P_N.

3.4. RSTC control system for the inverter

The proposed RSTC controller will monitor the amplitude, frequency, and phase angle of a grid power system. The control block diagram of the proposed RSTC controller is shown in Fig. 12. From *a-b-c* reference frame to *d-q* reference coordinate system, the phase angles of current and voltage are transformed by (37). The error is computed from the reference and measurement of *d-q* current, and the error in the *d-q* frame is given to proportional-integral (PI). The maximum value of the currently defined reference *d* and *q* component of the grid current controls grid power flow. It is only used for active power injection set to zero. The PI output is added to the feed-forward grid voltage component and decoupling component to generate the reference inverter output voltage. The output of PI regulator is converted to use (38) α-β frames. The reference frame of α-β and reference voltage of DC link voltage inverter SVPWM are used, and the switching signal is generated. The reference output voltage vector of the inverter (V_{ref}) is shown in Fig. 13. The reference voltage is the sum of components A and B. These values are used to determine the field of the reference voltage vector $V_{gd\mathrm{ref}}$ and $V_{gq\mathrm{ref}}$. The function of the vector angle is calculated in the below expression (37):

$$\begin{bmatrix} V_d \\ V_q \end{bmatrix} = \frac{2}{3} \begin{bmatrix} \cos\theta & \cos\left(\theta - \frac{2\pi}{3}\right) & \cos\left(\theta - \frac{4\pi}{3}\right) \\ -\sin\theta & -\sin\theta\left(\theta - \frac{2\pi}{3}\right) & -\sin\theta\left(\theta - \frac{4\pi}{3}\right) \end{bmatrix} \times \begin{bmatrix} V_{ga} \\ V_{gb} \\ V_{gc} \end{bmatrix}, \tag{37}$$

$$\begin{bmatrix} V_\alpha \\ V_\beta \end{bmatrix} = \begin{bmatrix} \cos\theta & -\sin\theta \\ \sin\theta & \cos\theta \end{bmatrix} \begin{bmatrix} V_d \\ V_q \end{bmatrix}. \tag{38}$$

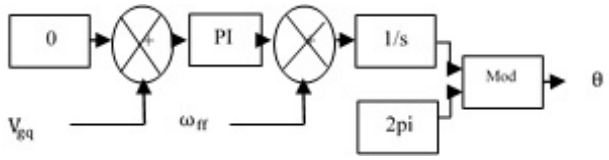

Fig. 13. The proposed RSTC controller phase angle gain block

The change in every 60 sectors with reference to such sectors of the vector, is determined based on the computed vector angle with calculate the zero time "T_0", where $T_0 = T_s - T_{\mathrm{eff}}$ is the time for which the switching vector is inactive for the state is 000 or 111. The inverter generates a combined voltage of zero vectors with two adjacent vectors.

The phase angle of the grid voltage is used to evaluate the RSTC controller, which is shown in Fig. 13. The grid angle is considered using the *q* component of grid voltage. The reference angle is set to zero, and the switching frequency of inverter is 20 kHz. The angular error is provided to the PI regulator and the angular frequency it produces. The PI output signal is added to the gate voltage to calculate the actual fundamental angular frequency. The frequency of the grid angle is obtained by the instantaneous phase angle.

The circuit topology modelled as a parameter analysis in Fig. 14. shows that assuming three-phase grid voltage is balanced when the switch is ideal, and the DC-link voltage is constant.

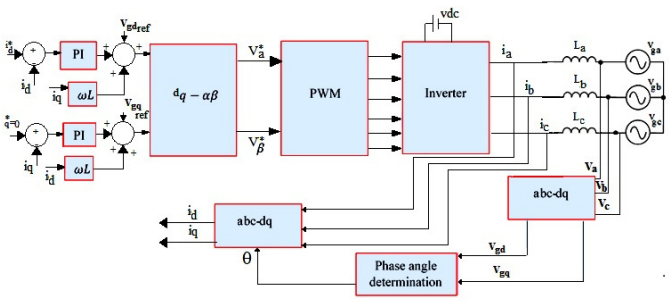

Fig. 12. Control block of the proposed RSTC

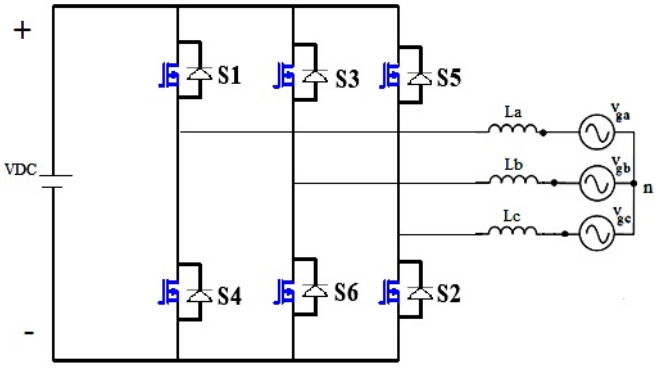

Fig. 14. Three-phase inverter circuit

$$V_d = L\frac{\mathrm{d}_{id}}{\mathrm{d}t} - \omega L i_q + V_{gd}\,, \tag{39}$$

$$V_q = L\frac{\mathrm{d}_{iq}}{\mathrm{d}t} - \omega L i_d + V_{gq}\,, \tag{40}$$

where V_d and V_q are the inverter output, i_d and i_q are the grid current, V_{gd} and V_{gq} are the grid voltage, ω is the grid frequency, and L_a, L_b, $L_c = L$ is the inverter output filter. This system is computed with a reference frame of *a*-*b*-*c* as given in (41)–(43) for each phase. The V_n is the function inverter output voltage by (41), which describes the leg switching states function, which is denoted in expression (43), are shown in Fig. 15.

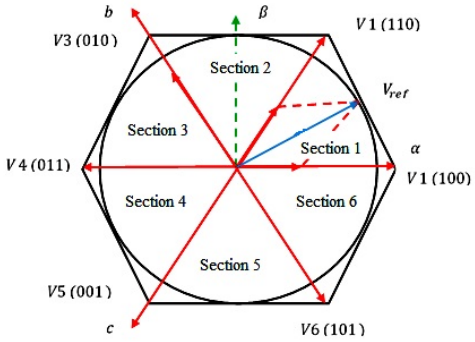

Fig. 15. Phase vector for RSTC

$$V_k = L\frac{\mathrm{d}_{ik}}{\mathrm{d}t} + V_{gk} + V_n\,, \tag{41}$$

$$V_n = \frac{1}{3}\left(V_a + V_b + V_c\right), \tag{42}$$

$$V_k = s_k V_{dc} = \begin{Bmatrix} V_{dc} & s_k = 1 \\ 0 & s_k = 0 \end{Bmatrix}. \tag{43}$$

In the above condition, k denotes to the inverter phase, and $K \in \{a, b,$ and $c\}$ and s characterize the condition of the upper switch. At the point when $S1$, $S2$, $S3$, $S4$, $S5$ and $S6$ are 1, the significant upper switch is ON and lower switch is OFF in the inverter switches.

3.4.1. RSTC algorithm

Step 1: Start.

Step 2: Initially, all the parameters and variables.

Step 3: Compute the solar power.

$$P_{pv} = V_{pv} \times I_{pv}\,. \tag{44}$$

Step 4: If the computed solar power is varied below the threshold region, the RSTC-MPPT regulates the PWM signal to the full bridge converter until the condition, $\left(\frac{\partial I_{pv}}{\partial V_{pv}}\right) + \left(\frac{I_{PV}}{v_{pv}}\right) = 0$ is satisfied.

Step 5: When solar power is adequate to provide a power supply to the inverter, $V_0 = V_{abc}$ the battery in discharging condition is stated by the RSTC controlling the switching operation of the bi-directional converter.

$$V_{L5} = -V_0 + V_{ba}\,. \tag{45}$$

Step 6: When solar power is not sufficient to provide power supply to the inverter, $V_0 \neq V_{abc}$ the battery in the charging condition.

$$V_{L5} = V_0 - V_{ba}\,. \tag{46}$$

Step 7: Sampling the reference phase voltage V_a, V_b and V_c to determine the switching time of the effective voltage vectors of different sectors, where T_s is the sampling period.

$$T_{as} = \frac{V_a \cdot T_s}{V_0} T_{bs} = \frac{V_b \cdot T_s}{V_0} T_{cs} = \frac{V_c \cdot T_s}{V_0}\,. \tag{47}$$

Step 8: Compute the value of T_{eff} (significant switching time). This is just the variance between maximum (maximum T_{as}, T_{bs} and T_{cs}) and minimum sample value. This is a sampled three-phase reference amplitude obtained after (T_{as}, T_{bs} and T_{cs}) and the three-component RSTC algorithm.

Step 9: Calculate the zero time "T_0", where $T_0 = T_s - T_{\text{eff}}$ is the time for which the switching vector is inactive for the state is 000 or 111. In that time T_{as}, T_{bs} and T_{cs} for the switching of the active switching vector of the corresponding sector.

Step 10: The time interval should be positive, so it shifts to the positive side by adding an offset. The offset time is evaluated as

$$T_{\text{offset}} = \frac{T_0}{2} - T_{\min}\,. \tag{48}$$

Step 11: This offset and on time intervals will be generated by the corresponding gate signal to the inverter. Therefore, the duration of the gate control signal of the different vector is obtained,

$$T_{Va} = T_{as} + T_{\text{offset}} T_{Vb} = T_{bs} + T_{\text{offset}} T_{Vc} = T_{cs} + T_{\text{offset}}\,. \tag{49}$$

The bottom switch is turned on for the rest of the sampling period.

Step 12: Step 11 is repeated for the switching of the active switching vector for all corresponding sectors.

Step 13: Stop the process.

The functional operation of the solar fed FBC with grid-connected inverter using the RSTC (RSTC) optimizer is given. The RSTC will be monitoring and controlling the full bridge converter voltage and the grid-connected inverter voltage.

4. RESULTS AND DISCUSSION

The proposed RSTC optimizer-based solar fed FBC with grid-connected inverter was developed using MATLAB-Simulink, which is represented in Fig. 16. In this work, the RSTC will be required to balance power and keep DC voltage constant under different lighting environments.

Table 1 describes the design parameters and the ranges of the proposed simulation model. Based on the above parameters, the proposed system will efficiently provide continuous power to the grid system.

The solar panel generate 41.2 V with the current of 8.3 A, when solar irradiance 1000 W/m^2 which is shown in Fig. 16. The obtained solar voltage will be given into the full bridge

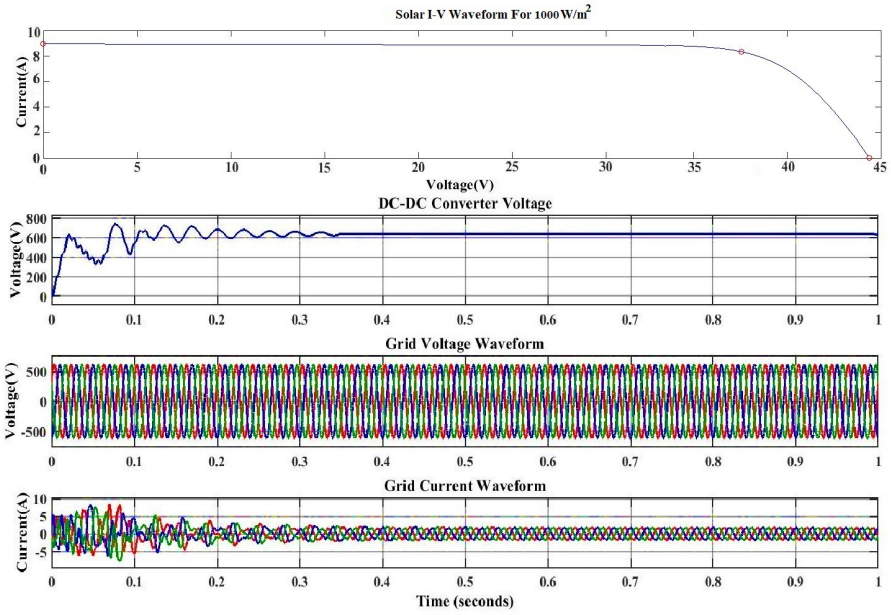

Fig. 16. Simulation waveform based on solar irradiance 1000 W/m^2

Table 1
Design parameters of the proposed simulation

Parameters	**Values**
Solar power (4 × 350) W Open circuit voltage (V_{OC}) for 350 Watts Short circuit current (I_{SC}) for 350 Watts	1400 W 44.51 V 10.5 A
Full bridge DC–DC converter output Converter switching frequency Converter switch Transformer turns ratio	650 V DC 5 kHz MOSFET 1:6
Inverter switching frequency Inverter switch	20 kHz IGBT
Grid voltage Grid current	440 V AC 5 A
Grid frequency	50 Hz
i. Bi-directional converter for battery charging mode ii. Discharging mode iii. Buck-boost converter Switching frequency	12 V 150 Ah 620 V 150 Ah 5 kHz
iv. Charging current and discharging current values v. Inductor L_1, L_o and 3 capacitors values	Discharging current value is 7.5 A $L_1 = 10\text{E}{-2}$ H $L_o = 0.3\text{E}{-6}$ H $C_1 = 0.01\text{E}{-3}$ F $C_2 = 0.07\text{E}{-3}$ F $C_3 = 1\text{E}{-3}$ F
AC Load (3Φ Resistive)	1 kΩ

converter for stability voltage. Due to some low level of solar voltage, the proposed RSTC controller will regulate the duty cycle of the FBC $DT_s = t, t+1, t+2, \ldots, t+n$ based on duty cycle variation, the converter will stabilize the 620 V. The stable DC voltage is provided to the inverter, which will convert DC–AC. The proposed RSTC controller will provide the AC power to the grid with fewer distortions.

The above Fig. 17 shows the solar irradiance 500 W/m^2. The solar panel will generate the 38.5 V with a current value of 7.6 A based on the irradiance. In this state, the solar voltage will not meet the required power, which is needed for the inverter. Due to this condition, the proposed RSTC-MPPT system will measure the solar power curve alienated in two sides, left and right side MPPT. The variation in current and voltage are analyzed to get closer to the point of operation. If the generated solar voltage is unequal to the VI operating point, the RSTC controller varies the duty cycle ration $DT_s = t, t+1, t+2, \ldots, t+n$. The compensated and improved solar DC voltage 620 V is fed to the inverter for DC–AC conversion. Finally, converted AC voltage is fed to the grid system.

Based on the solar irradiance 200 W/m^2 the solar panel will generate the 37.4 V with the current value of 5.7 A, which is shown in Fig. 18. Due to the low irradiance, the generation of the solar voltage is also low, also the converter output has more distortion in the initial time (0–0.17) s. During this mentioned period, the RSTC controller will regulate the input voltage but is not adequate to stabilize the voltage or meet the required voltage at the time duration. To attain the required voltage 620 V, the RSTC-MPPT regulates the PWM signal to the full bridge converter until the condition, $\left(\frac{\partial I_{pv}}{\partial V_{pv}}\right) + \left(\frac{I_{PV}}{v_{pv}}\right) = 0$ is satisfied. Finally, the stabilized voltage will be achieved at the time of 0.4 s, which is clearly represented in Fig. 18.

The BESS is utilized under necessary conditions. When the solar panel generates low power, the battery is on a discharging state from the time of 0–0.1 s. When the solar voltage is increased, the battery will go to the charging mode which is shown in Fig. 19. The proposed RSTC control-based bi-

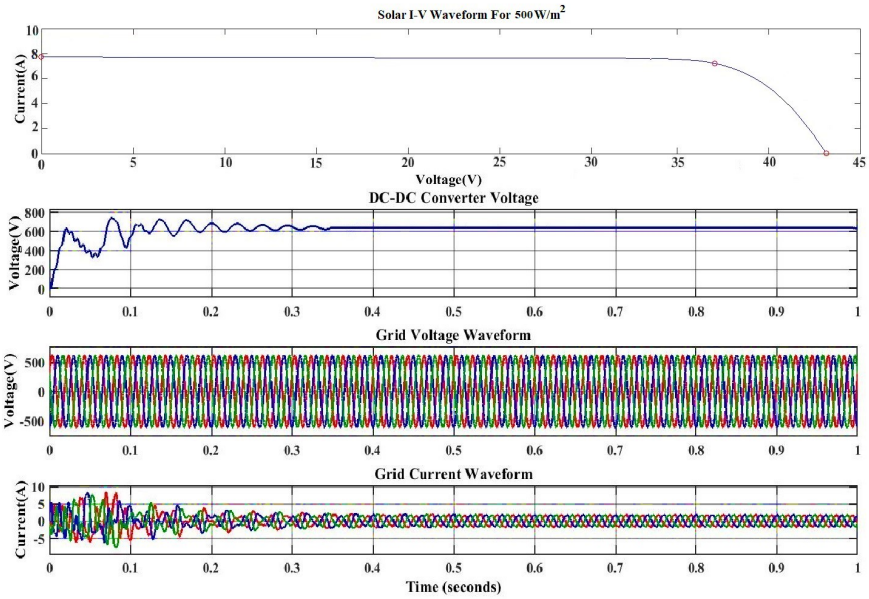

Fig. 17. Simulation waveform based on solar irradiance 500 W/m^2

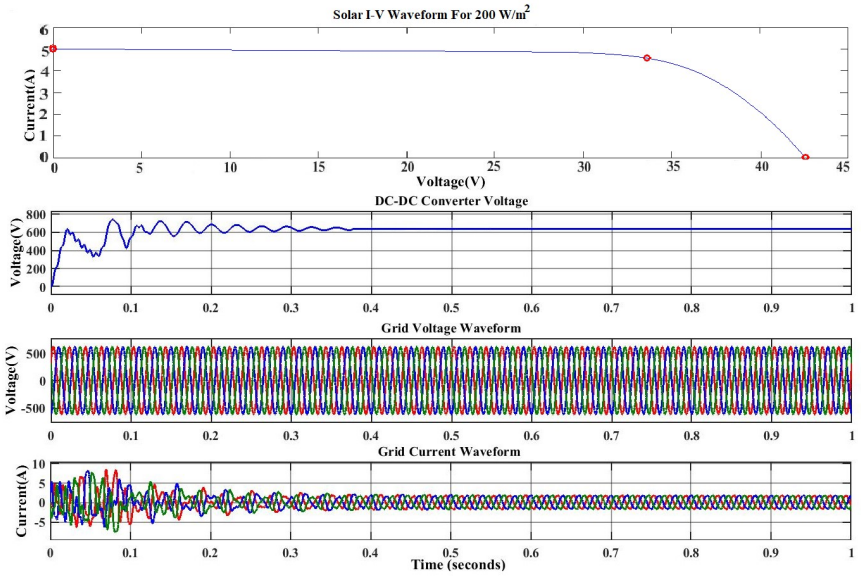

Fig. 18. Simulation waveform based on solar irradiance 200 W/m^2

directional converter will operate in two modes of operation (i) charging mode, (ii) discharging mode; both of these mode operations are based on the solar power generation.

Table 2 represents the performance analysis of the proposed system based on steady-state error, THD and overall efficiency.

Table 2
Performance analysis of the proposed system

Methods	Steady state error (per unit)	THD (%)	Efficiency (%)
PID [31]	0.856	7.23	88.7
RSTC	0.27	2.88	91.4

Steady-state error for full bridge converter:

The feedback control system is used to compensate the unnecessary input signals and compensate for the system.

$$e_c(t) = \frac{\text{Estimated output}}{\text{Number of the deviated output of the converter}}, \tag{50}$$

where, $e_c(t)$ is a system error.

Voltage deviation in the converter output = 320 + 680 + 640 + 630 = 2270 V,

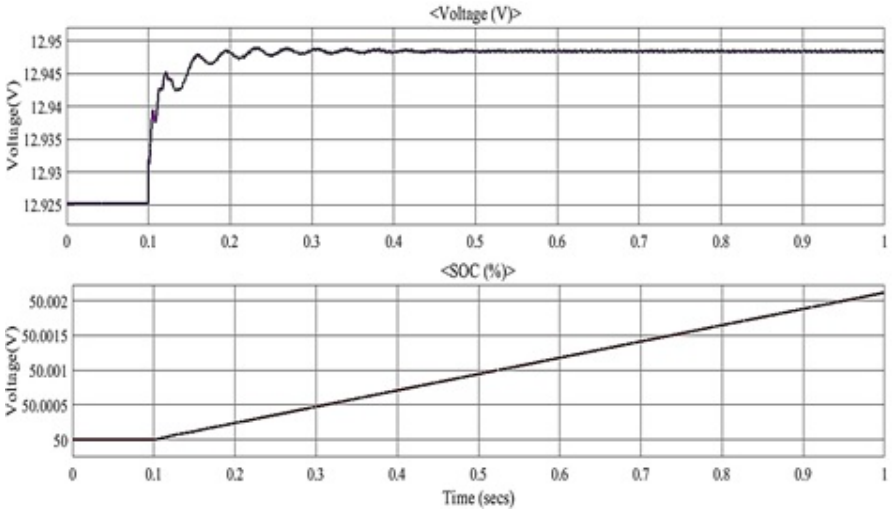

Fig. 19. Simulation waveform for battery

$$\text{Estimated output} = 620\ \text{V},\ e_c(t) = \frac{620}{2270} = 0.27,$$

$$\text{THD}(\%) = \frac{\sum_{n=2}^{\infty} \text{harmonics} + \text{noise}}{\text{fundamental}}. \tag{51}$$

Efficiency formula for the FBC:

$$\eta(\%) = \frac{\text{Maximum possible output}}{\text{Actual Input}} \times 100\%. \tag{52}$$

Actual input power = 1400 W,
Number of solar panels = 4,
One solar panel rating = 350 W,
Maximum possible output = 620 V ×2.06 A = 1280 W,

$$\eta(\%) = \frac{1280}{1400} \times 100\% = 0.914 \times 100\%,$$

Efficiency = 91.4%.

5. CONCLUSION

This system utilizes the RSTC optimizer for solar fed FBC and grid-connected inverter for effective energy management systems in smart grid application. The simulation has been done with FBC and tested with different light conditions. The simulation results provide the guidelines to keep up the parameters of solar power generation with BESS. The purpose of this system is to decrease operating costs and environmental impact of micro grids, which will increase the efficiency of power generation system. The primary purpose of full bridge converter is to stabilize the solar power and provide constant input for the grid-connected inverter. The proposed RSTC method utilizes the active tracking of the maximum potential in the MPP system, which will initially improve solar power stability. The FBC will be operated in four modes, to maintain required output voltage at 620 V. Based on the modes of operation, the solar voltage will be improved by reducing the switching stress of the FBC. A constant switching frequency of 5 kHz is applied to the converter switches, which diminishes the distortion in the converter output.

The second stage is the function of the inverter using RSTC. To ensure efficient use of grid-connected solar power, the inverter is designed with energy conversion and adaptation functions between the source and the grid voltage. The RSTC controller analyses the difference between vector voltages and respective reference voltages at the sampling period. The RSTC will maintain PWM of the inverter, if the inverter output voltages are equal to grid voltages; otherwise, the gate control signal varied at different vector voltage is obtained from the inverter. To reduce the total harmonics distortion and switching stress of the inverter, the 20 kHz constant switching frequency is applied. Due to this function, the system's overall power quality will be improved.

The third stage of the process is battery management for the continuous power delivery to the grid system. The bi-directional converter-based BESS is used. The main goal of this system is to deliver power only when it is extremely necessary. The bi-directional converter performs charging /discharging of battery. During the charging condition, it will work in the buck mode to maintain 12 V for charging the battery. If the solar power output reduces to the value between (0-8) V, the RSTC controller provides the modified switching operation of the bi-directional converter. During this condition, the converter operates in boost mode while maintaining the 620V in the DC bus system. The RSTC technique will maintain and control the battery power. The proper implementation of all three stages attains high-performance converter and inverter with fast dynamic response with low THD and pure sine wave in inverter output voltage, which is more suitable for stability solar power generation based grid-tie applications. The proposed RSTC technique will monitor and control all the proposed model parameters. This work's main contribution is to maintain the output voltage at different solar irradiance and quick

energy compensation of the system. The RSTC optimizer control ensures energy management between renewable energy and the grid power system. The simulation results confirmed that the proposed RSTC controller has attained high operating performance with the evaluated parameters like steady-state condition 0.27(per unit) and THD of 2.88 (%), which is low when compared with the conventional PID control technique.

REFERENCES

[1] S. Chakraborty, and S. Chattopadhyay, "A Dual-Active-Bridge-based Novel Single-stage Low Device Count DC–AC Converter," *IEEE Trans. Power Electron.*, vol. 34, no. 3, pp. 2339–2354, Mar. 2018.

[2] D. Sha, J. Zhang, and T. Sun, "Multi-Mode Control Strategy for SiC MOSFETs Based Semi Dual Active Bridge DC–DC Converter," *IEEE Trans. Power Electron.*, vol. 34, no. 6, pp. 5476–5486, June, 2019.

[3] G. Xu, D. Sha, Y. Xu, and X. Liao, "Dual-Transformer-Based DAB Converter with Wide ZVS Range for Wide Voltage Conversion Gain Application," *IEEE Trans. Ind. Electron.*, vol. 65, no.4, pp. 3306–3316, Apr. 2018.

[4] D. Sha, X. Wang, K. Liu, and C. Chen, "A Current-Fed Dual Active Bridge DC–DC Converter Using Extended Duty Cycle Control and Magnetic-Integrated Inductors With Optimized Voltage Mismatching Control," *IEEE Trans. Power Electron.*, vol. 34, no. 1, pp. 462–473, Jan. 2019.

[5] S. Samanta and A.K. Rathore, "Wireless power transfer technology using full-bridge current-fed topology for medium power applications," *IET Power Electron.*, vol. 9, no. 1, pp. 1903–1913, Jul. 2016

[6] P. Li, G.P. Adam, D. Holliday, and B. Williams, "Controlled Transition Full-Bridge Hybrid Multilevel Converter with Chain-Links of Full-Bridge Cells," *IEEE Trans. Power Electron.*, vol. 32, no. 1, pp. 23–38, Jan. 2017.

[7] A.J.B. Bottion, and I. Barbi, "Input-Series and Output-Series Connected Modular Output Capacitor Full-Bridge PWM DC–DC Converter," *IEEE Trans. Ind. Electron.*, vol. 62, no. 1, pp. 6213–6221, Oct. 2015.

[8] L. Wang and T. Zhang, "System performance analysis of the input-parallel and output-series full-bridge converters considering parameter difference," *3rd International Conference on Electronics Computer Technology*, April 2011, pp. 177–181.

[9] Z. Zhang, O.C. Thomsen, and M.A.E. Andersen, "Soft-Switched Dual-Input DC–DC Converter Combining a Boost-Half-Bridge Cell and a Voltage-Fed Full-Bridge Cell," *IEEE Trans. Power Electron.*, vol. 28, no. 11, pp. 4897–4902, Nov. 2013.

[10] E. Sunan, F. Kucuk, H. Goto, H.J. Guo, and O. Ichinokura, "Three-Phase Full-Bridge Converter Controlled Permanent Magnet Reluctance Generator for Small-Scale Wind Energy Conversion Systems," *IEEE Trans. Energy Convers.*, vol. 29, no. 3, pp. 585–593, Sep. 2014.

[11] M. Narimani, and G. Moschopoulos, "An Investigation on the Novel Use of High-Power Three-Level Converter Topologies to Improve Light-Load Efficiency in Low Power DC/DC Full-Bridge Converters," *IEEE Trans. Ind. Electron.*, vol. 61, no. 10, pp. 5690–5692, Oct. 2014.

[12] C. Liu *et al.*, "High-Efficiency Hybrid Full-Bridge–Half-Bridge Converter with Shared ZVS Lagging Leg and Dual Outputs in Series," *IEEE Trans. Power Electron.*, vol. 28, no. 2, pp. 849–861, Feb. 2013.

[13] G. Li, J. Xia, K. Wang, X. He, and Y. Wang, "Hybrid Modulation of Parallel-Series LLC Resonant Converter and Phase-Shift Full-Bridge Converter for A Dual Output DC–DC Converter," *IEEE J. Emerging Sel. Top. Power Electron.*, vol. 7, no. 2, pp. 833–842, Jun. 2019.

[14] M.R. Yazdani, and M. Farzanehfard, "Evaluation and Comparison of Conducted EMI in Three Full-Bridge DC–DC Switching Converters," *10th International Power Electronics, Drive Systems, and Technologies Conference (PEDSTC)*, Feb. 2019.

[15] J.W. Kim, D.Y. Kim, C.E. Kim, and G.W. Moon, "A Simple Switching Control Technique for Improving Light Load Efficiency in a Phase-Shifted Full-Bridge Converter with a Server Power System," *IEEE Trans. Power Electron.*, vol. 29, no. 4, pp. 1562–1566, Apr. 2014.

[16] G. Guo *et al.*, "Series-connected-based Offshore Wind Farms with Full-bridge Modular Multilevel Converter as Grid and Generator-side Converters," *IEEE Trans. Ind. Electron.*, vol. 67, no. 4, pp. 2798–2809, Apr. 2020.

[17] U. Kundu, K. Yenduri, and P. Sensarma, "Accurate ZVS Analysis for Magnetic Design and Efficiency Improvement of Full-Bridge LLC Resonant Converter," *IEEE Trans. Power Electron.*, vol. 32, no. 3, pp. 1703–1706, Aug. 016.

[18] R. Adle, M. Renge, and S. Muley, "Improvement in Performance of Series Z-source Inverter with an Application as Solar PV Fed Water Pump," *Iran. J. Sci. Technol. Trans. Electr. Eng.*, vol. 44, pp. 1263–1279, Jan. 2020, doi: 10.1007/s40998-020-00310-y.

[19] L.J. Jeremy, C.A. Ooi, and J. Teh, "Non-isolated conventional DC–DC converter comparison for a photovoltaic system: A review," *J. Renewable and Sustainable Energy*, vol. 12, no. 1, p. 013502, Jan. 2020.

[20] C. Bai, B. Han, and M. Kim, "Current-fed dual-half-bridge converter directly connected with half-bridge inverter for a residential photovoltaic system," *Solar Energy*, vol. 174, pp. 108–120, Nov. 2018.

[21] W. Xu, A. Li, Y. Su, M. Zhu, X. Ouyang, and X. Yang, "Optimal Expansion Planning of AC/DC Hybrid System Integrated with VSC Control Strategy," *IEEE Innovative Smart Grid Technologies – Asia (ISGT Asia)*, China, May 2019, doi: 10.1109/isgt-asia.2019.8881734.

[22] X. Liu, and Y. Liu, "Optimal planning of AC-DC hybrid transmission and distributed energy resource system: Review and prospects," *CSEE J. Power Energy Syst.*, vol. 5, no. 3, pp. 409–422, Sep. 2019.

[23] M. Shojaie, and O.A. Mohammed, "A Multi-input DC–DC Converter with AC-DC PFC Buck-boost Stage for Hybrid Energy Storage Systems," *SoutheastCon 2018*, USA, April 2018, doi: 10.1109/secon.2018.8478879.

[24] R. Barrera-Cardenas, O. Mo, and G. Guidi, "Optimal Sizing of Battery Energy Storage Systems for Hybrid Marine Power Systems," *IEEE Electric Ship Technologies Symposium (ESTS)*, Washington, USA, Aug. 2019, doi: 10.1109/ests.2019.8847932.

[25] Z. Zheng, J. Zheng, W. Zhao, and Z. Han, "Research on Dynamic Voltage Characteristics of AC/DC Hybrid System Based on PET," *IEEE Innovative Smart Grid Technologies – Asia (ISGT Asia)*, China, May 2019, doi: 10.1109/isgt-asia.2019.8881201.

[26] S. Farhangi, A. Nazer, G.R. Moradi, and E. Asadi, "Improved Performance of Solar Array Simulator Based on Constant Voltage/Constant Current Full-Bridge Converter," *11th Power Electronics, Drive Systems, and Technologies Conference (PEDSTC)*, Tehran, Iran, Feb. 2020, doi: 10.1109/PEDSTC49159.2020.9088485.

[27] D. Sha, J. Zhang, and T. Sun, "Multi-Mode Control Strategy for SiC MOSFETs Based Semi Dual Active Bridge DC–DC Converter," *IEEE Trans. Power Electron.*, vol. 34, no. 6, pp. 5476–5486, June 2019.

[28] G. Xu, D. Sha, Y. Xu, and X. Liao, "Dual-Transformer-Based DAB Converter with Wide ZVS Range for Wide Voltage Conversion Gain Application," *IEEE Trans. Ind. Electron.*, vol. 65, no. 4, pp. 3306–3316, April 2018.

[29] D. Debnath and K. Chatterjee, "Two-Stage Solar Photovoltaic-Based Stand-Alone Scheme Having Battery as Energy Storage Element for Rural Deployment," *IEEE Trans. Ind. Electron.*, vol. 62. no. 7, pp. 4148–4157, July 2015.

[30] B. Mangu, S. Akshatha, D. Suryanarayana, and B.G. Fernandes, "Grid-Connected PV-Wind-Battery-Based Multi-Input transformer-coupled Bidirectional DC–DC Converter for Household Applications," *IEEE J. Emerging Sel. Top. Power Electron.*, vol. 4, no. 3, pp. 1086–1095, Sep. 2016.

[31] M.-K. Nguyen, T.-D. Duong, "Isolated Boost DC–DC Converter with Three Switches," *IEEE Trans. Power Electron.*, vol. 33, no. 2, pp. 1389–1398, Feb. 2018.

[32] G. Ning, B. Fang, D. Qin, Y. Liang, and L. Zheng, "Design and application of comprehensive evaluation index system of smart grid based on coordinated planning of major network and power distribution network," *Arch. Electr. Eng.*, vol. 70, no. 1, pp. 103–113, 2021, doi: 10.24425/aee.2021.136055.

[33] M. Bobrowska-Rafal, K. Rafal, M. Jasinski, and M. Kazmierkowski, "Grid synchronization and symmetrical components extraction with PLL algorithm for grid connected power electronic converters – a review," *Bull. Pol. Acad. Sci.: Tech. Sci.*, vol. 59, pp. 485–497, Dec. 2011, doi: 10.2478/v10175-011-0060-8.

[34] J. Bindu, S. Selvaperumal, S. Muralidharan, and M. Muhaidheen, "Genetic algorithm based Selective Harmonic Elimination in PWM AC-AC converter," *International Conference on Recent Advancements in Electrical*, *Electronics And Control Engineering*, Dec. 2011, pp. 393–397, doi: 10.1109/ICONRAEeCE.2011.6129809.

[35] S. Selvaperumal and C.Ch.A. Rajan, "Micro-Controller Based LCCResonantConverterAnalysis, Design, and Simulation Results.," *Int. J. Comput. Electr. Eng.*, vol. 1, no. 3, pp. 323–327, Aug. 2009.

[36] S. Selvaperumal *et al.*, "Performance investigation of SHE PWM implementation of GA based LCL resonant inverter in marine applications," *Ind. J. Geo Mar. Sci.*, vol. 46, no. 9, pp. 1889–1898, Sep. 2017.

[37] S. Selvaperumal, C.Ch.A. Rajan, "Investigation of Fuzzy Control Based LCL Resonant Converter in RTOS Environment," *J. Intell. Fuzzy Syst.*, vol. 26, no. 2, pp. 913–924, Jan. 2014.

[38] W. Kolodziejczyk, I. Zoltowska, and P. Cichosz, "Real-time energy purchase optimization for a storage-integrated photovoltaic system by deep reinforcement learning," *Control Eng. Pract.*, vol. 106, p. 104598, Jan. 2021.